arXiv:cond-mat/0005153v1 [cond-mat.mtrl-sci] 9 May 2000

Electronic structure of Co_xTiSe_2 and Cr_xTiSe_2

A. N. Titov, A. V. Kuranov, and V. G. Pleschev
Ural State University, Physics of Condensed Matter Department, 620083 Yekaterinburg, Russia

Yu. M. Yarmoshenko and M. V. Yablonskikh
Institute of Metal Physics, Russian Academy of Sciences-Ural Division, 620219 Yekaterinburg GSP-170, Russia

A. V. Postnikov
Theoretical Low-Temperature Physics, University of Duisburg, D-47048 Duisburg, Germany

S. Plogmann and M. Neumann
Department of Physics, Osnabrück University, D-49069 Osnabrück, Germany

A. V. Ezhov and E. Z. Kurmaev
Institute of Metal Physics, Russian Academy of Sciences-Ural Division, 620219 Yekaterinburg GSP-170, Russia

(November 13, 2018)

The results of investigations of intercalated compounds Cr_xTiSe_2 and Co_xTiSe_2 by X-ray photoelectron spectroscopy (XPS) and X-ray emission spectroscopy (XES) are presented. The data obtained are compared with theoretical results of spin-polarized band structure calculations. A good agreement between theoretical and experimental data for the electronic structure of the investigated materials has been observed. The interplay between the $M3d$–Ti$3d$ hybridization (M=Cr, Co) and the magnetic moment at the M site is discussed. A 0.9 eV large splitting of the core Cr$2p_{3/2}$ level was observed, which reveals a strong exchange magnetic interaction of 3d-2p electrons of Cr. In the case of a strong localization of the Cr$3d$ electrons (for $x < 0.25$), the broadening of the CrL spectra into the region of the states above the nominal Fermi level was observed and attributed to X-ray re-emission. The measured kinetic properties are in good accordance with spectral investigations and band calculation results.

71.20.-b 71.20.Tx 72.80.Ga 78.70.En 79.60.-i

I. INTRODUCTION

Intercalated compounds built by insertion of transition metal (TM) atoms into layered titanium dichalcogenides are interesting as natural nanostructures formed by alternation of magnetic TM layers and non-magnetic layers of the host lattice. The investigations performed for M_xTiS_2 (M = Mn, Fe, Co, Ni) [1–3] show that the effect of intercalation on the chemical bonding is not consistent with the rigid band model [4] often referred to in relation to these compounds. Instead, the charge carriers localization due to the formation of covalent bonds with intercalant atoms seems to become important. From this point of view, the $TiSe_2$-based intercalated materials are obviously even more interesting, because they demonstrate a higher degree of two-dimensionality in comparison with TiS_2, as follows from their larger c/a ratio (1.697 in pure $TiSe_2$ vs. 1.672 in TiS_2, see, e.g., Ref. [5]). Tazuke *et al.* [6] discussed magnetic properties of M_xTiSe_2 (M = V, Cr, Mn, Fe, Co, Ni, Cu) referring to the hybridization between the intercalant $3d$ states and the band states of $TiSe_2$, the information on the latter being based on the band structure calculation [7]. According to Ref. [7], the hybridized states with lighter TM atoms have smaller contribution of Se$4p$ states.

The aim of the present work is to deepen the understanding of the chemical bonding and related (magnetic and transport) properties of two $TiSe_2$-based systems, intercalated with "light" (Cr) and "heavy" (Co) TM atoms. Monocrystalline samples over a range of intercalant concentration were prepared and used in the study of magnetic susceptibility, conductivity, X-ray emission and photoelectron spectroscopy.

While for the system Co_xTiSe_2 the literature data about influence of intercalation on crystal structure [8], electric and magnetic properties [9] were reported earlier, for Cr_xTiSe_2 system we failed to find any literature data except those of Ref. [6].

II. EXPERIMENTAL

Polycrystalline Co_xTiSe_2 and Cr_xTiSe_2 samples ($0 < x < 0.5$) were prepared by an ampoule synthesis method from the constituent elements. The methods of synthesis and characterization are described in detail in Ref. [9]. The initial diffraction data were obtained with a DRON 1UM diffractometer (Cu $K\alpha$, Ni filtered radiation.) The unit cell parameters have been then determined by a least square refinement with 16 reflexes with the accuracy $\Delta a_0 = \pm 0.001$, $\Delta c_0 = \pm 0.002$ Å. The hexagonal unit cell parameters of intercalated $TiSe_2$ are shown in Fig. 1. The crystal structure, electric and magnetic properties of Co_xTiSe_2 are described in Refs. [8,9]. The information about the type of intercalant ordering in Co_xTiSe_2 is controversial [8], which may be traced back to different thermal treatments of the samples. In the present work we used the samples quenched from 850 °C in ice water. For the samples so prepared, no ordering of intercalant atoms was observed in both systems.

At temperatures above that of liquid nitrogen, both materials are paramagnetic, with a temperature dependence of their magnetic susceptibility following a Curie-Weiss law. The values of effective magnetic moments are close to nominal spin moments of Co^{2+} and Cr^{3+} ions, respectively.

The single crystals for the X-ray spectra measurements were grown by the gas transport reaction method in evacuated quartz ampoules with I_2 as gas-carrier [10]. Powdered $Co_{0.25}TiSe_2$ and $Cr_{0.25}TiSe_2$ material was used as origin materials. In the case of $Co_{0.25}TiSe_2$ there was a flow of substance from the hot (1000 °C) to the cold (600 °C) edge of the ampoule. The single crystals had a shape of thin plates ≈ 2-3 mm large and ≈ 0,1 mm thick. The final intercalant content (determined from the lattice parameter values) was found to be close to the initial one: $Co_{0.23}TiSe_2$. In the case of $Cr_{0.25}TiSe_2$ the substance was transferred from the middle part (at 900 °C) where the powder was initially placed to both hot (1100 °C) and cold (700 °C) edges of the ampoule. The single crystals grown at the hot edge of the ampoule had a shape of slim needles with the size close to 0.3×0.1×10 mm, whereas those grown at the cold edge were thin plates 2–4 mm large and ≈0.1 mm thick. From the unit cell parameters comparison we found that the crystals formed at the cold edge have the composition $Cr_{0.1}TiSe_2$, those at the hot edge – $Cr_{0.5}TiSe_2$.

The X-ray photoelectron spectroscopy (XPS) measurements were performed at a Perkin Elmer spectrometer with an energy resolution of 0.3 eV, X-ray emission spectroscopy (XES) measurements – at a soft X-ray radiation spectrometer RSM-500 with electron excitation and an energy resolution of 0.7 eV. The single crystals of $Co_{0.23}TiSe_2$ and $Cr_{0.1}TiSe_2$ were cut by a razor blade in the spectrometer chamber directly before the measurements.

III. CRYSTAL STRUCTURE AND BULK PROPERTIES

In this section, we present the discussion of the electronic characteristics as they might be deduced from the analysis of the measured bulk properties. The microscopic aspects of hybridization will be discussed in Sec. V in relation with *ab initio* calculations. A decrease of the lattice parameter c in the course of intercalation is typical for M_xTiSe_2 systems as has been mentioned in Ref. [8,10] and could be seen in Fig. 1. This might be understood as a result of covalent bonds being formed between intercalant atoms and the host lattice [11]. While free Co^{2+} and Cr^{3+} ions have the same spin value of 3/2, in intercalated systems the experimentally obtained effective magnetic moment at the Cr atom is roughly 1.5 times larger than that per Co atom (see Table I). This fact may be related to a stronger hybridization of $3d_{xz,yz}$ orbitals (those participating in the magnetic moment formation in the $3d^7$ configuration of Co^{2+}) with the Se4p orbitals. In contrast, the $3d_{xz,yz}$ orbitals are essentially empty in the $3d^3$ configuration of Cr^{3+}. The deviation of the effective moment from its nominal free-ion value correlates well with the lattice distortion (which is the measure of the chemical bonding between an intercalant and the host [11]) at least for concentrations $x \leq 0.25$ as is shown in Fig. 2. The systems with $x = 0.33$ are actually beyond the percolation limit on the ordered lattice of $3d$ "impurities", so that their clustering and direct exchange interaction apparently results in the drop of magnetic moments and breakdown of the abovementioned correlation.

The lattice deformation and change in the degree of hybridization affects the conductivity σ of the M_xTiSe_2 systems. While in Co_xTiSe_2 σ is only weakly concentration-dependent, in Cr_xTiSe_2 it exhibits an interesting behavior – being on the average higher, $\sigma(x)$ includes several irregularities. Fig. 3 shows the conductivity at room temperature, but the irregularities persist over a broad temperature range. Two different types of $\sigma(T)$ are shown in the inset of Fig. 3 for two Cr concentrations.

An overall decrease of σ as the unit cell parameter c decreases (see Fig. 3) is apparently due to the drop in the free charge carriers concentration as electrons are trapped in covalent bonds – this seems to be well the case at least in all Co-containing systems. Due to a different charge configuration of Cr^{3+} as compared to Co^{2+}, one electron provided by Cr remains free and contributes to the metallic type of conductivity – see the calculated density of states (DOS) distribution at the impurity site, Sec. V. A drop in the conductivity near x=0.05 of Cr probably indicates the compensation of highly mobile intrinsic (hole-type) carriers in $TiSe_2$, the concentration of which is 0.05 per

formula unit [12]. This is consistent with a perfectly metallic type of temperature dependency of conductivity for this concentration, as shown in the inset of Fig. 3. Another drop in $\sigma(x)$ at x=0.25 may be related to the percolation limit on a lattice of those Ti atoms which have no Cr neighbors. Two Ti atoms (to both sides of the intercalated Cr atom) participate in the formation of localized bonds, and the percolation limit for two-dimensional hexagonal lattices equals 0.5 [13]. For x=0.33, differently from lower Cr concentrations, the activation region is seen (inset in Fig. 3) in the $\sigma(T)$, indicating an opening of the band gap at the Fermi level. It is noteworthy that at x=0.33, exactly one extra electron is provided by Cr per titanium atom. One can speculate that the gap formation is the consequence of spin splitting of the Cr-Ti hybridized band, since this band could exactly accommodate one electron per Ti atom. No such gap is seemingly formed in Co_xTiSe_2, presumably because more efficient deformation of the host lattice results in more octahedral coordination of Ti atoms by chalcogen, preventing the splitting between d_{z^2} and d_{xy}, $d_{x^2-y^2}$ orbitals of Ti [14].

IV. X-RAY PHOTOELECTRON AND X-RAY EMISSION SPECTRA

We refer to the XPS spectra with three main purposes: to control the quality of monocrystalline samples, to get information about the electronic structure and to trace the effects of on-site magnetic interactions on the spectra. Figs. 4 and 5 depict the 2p core levels of titanium and of intercalated elements, correspondingly. Ti 2p spectra are known to exhibit relatively large chemical shifts already at early oxidation states (see, e.g., [15]). The actual spectra indicate a good (oxygen-free) quality of samples. The chemical shift still present (455.0 eV for the Ti2$p_{3/2}$ binding energy in $TiSe_2$; 455.5 eV in $Co_{0.5}TiSe_2$; 455.8 eV in $Cr_{0.1}TiSe_2$) exhibits the increase of ionicity from the host to Co-based to Cr-based systems [16]. This is consistent with above discussed (Fig. 1) stronger z-contraction of the crystal lattice in more covalent Co_xTiSe_2, as compared to Cr_xTiSe_2.

Of interest are the core 2p photoemission spectra of intercalant atoms, which may exhibit an exchange splitting due to an intra-atomic 2p–3d interaction (similarly to what has been demonstrated for the Mn-based Heusler alloys [17,18]). As is seen in Fig. 5, the Cr2$p_{3/2}$ line in $Cr_{0.1}TiSe_2$ clearly shows a splitting of about 1 eV, differently from the Co2$p_{3/2}$ spectrum of $Co_{0.23}TiSe_2$ where no such splitting is observed. The splitting is qualitatively related to the difference between local magnetic moments in these compounds (see Table I).

The valence-band (VB) photoelectron spectra (Fig. 6) have a relatively simple structure, where the Se4s contribution (in the region of binding energies 12–16 eV) is clearly separated from the Se4p–Ti3d–M3d hybridized band spanning the binding energies 0–6 eV. In the latter band, the contribution from the Se4p states is the most pronounced, since the photoionization cross-section of selenium is much larger than for all other constituents [19]. However, the contribution of Cr3d and, in particular, Co3d states is noticeable just below the Fermi energy, similarly to the behavior detected for the Fe3d states in Fe_xTiTe_2 [11]. An analysis of the calculated DOS (see next section) shows that a narrow peak at ≈1.5 eV below the Fermi level, well separated from the bulk of Se4p states, indeed dominates the local DOS at the Co site and must be visible in the valence-band XPS.

The trends in the "local" electronic structure of intercalant atoms depending on concentration are much better visible from X-ray emission spectra which are element-selective and hence not masked by the contributions from selenium states. The Cr and Co $L_{\alpha,\beta}$ spectra ($4s3d \rightarrow 2p_{3/2,1/2}$ transitions) have been measured for several concentrations and are shown in Fig. 7. Based on the arguments of Ref. [20], the concentration-related differences in the spectra can be traced to the percolation threshold on a two-dimensional hexagonal lattice at $x = 0.25$. Above this threshold, the intercalant atoms (under an uniform distribution) may have a neighbor of the same type at the distance of hexagonal lattice constant. It is noteworthy how the width and the relative intensity of L_α and L_β bands vary with the concentration. The Cr $L_{\alpha,\beta}$ spectra of intercalated compounds are quite different from those of pure metallic Cr, whereas the corresponding differences for the Co-based systems are less pronounced.

A striking difference in the XES of Co- and Cr-intercalated systems is a much broader emission band in the latter, in spite of the fact that the widths of the occupied valence bands in both systems are presumably not too much different. The shift of the X-ray emission spectra by the 2$p_{3/2}$ core level binding energy onto the common energy scale with the XPS (Fig. 6) makes obvious that the states above the nominal Fermi level effectively participate in the emission process in $Cr_{0.1}TiSe_2$, but not in Co-intercalated systems. Another peculiarity of the spectra shown in Fig. 7 is the increase of the L_β/L_α relative intensity in more diluted (especially in Cr-based) systems. The broadening of L_α spectra of 3d components has been detected and discussed before – in 3d oxides (of Mn [21,22] and Cu [23]) where charge-transfer excitations were argued to be an important mechanism responsible for a rich satellite structure, as well as in pure 3d metals (Cu, [24]) where an initial-state 3d vacancy satellite was shown to contribute on the high-energy side of the L_α line for excitation energies beyond the L_2 threshold. For our systems in question, none of these mechanisms seem to work: charger-transfer excitations cannot play an important role because of a much high covalency than in oxides; as for shake-up/shake-off processes – it is difficult to argue why their intensity would be

enhanced at low Cr (but not Co) concentrations. Moreover, the increase of the high-energy satellite in Cu $L_{\alpha,\beta}$ in Ref. [24] is accompanied by the decrease of the L_β/L_α intensity ratio (due to the Coster-Kronig process) – the trend opposite to that observed in the present case.

What makes the difference between low-concentrartion Cr-intercalated system and other systems studied is relatively high localization of the Cr3d state and high magnetic moment associated with it. It is noteworthy that in recently studied Heusler alloys NiMnSb and Co_2MnSb where the high magnetic moment at the Mn site is similarly localized, the L_α emission from the states nominally above the Fermi level was observed [25]. Similarly to how it was argued in Ref. [25] for Heusler alloys, we tend to qualitatively attribute the anomalous X-ray emission in the diluted Cr_xTise_2 system to a relaxation of the intermediate state with electronic configuration $2p^5 3d^{n+1}$, which involves the contribution from the states of d symmetry nominally vacant in the ground-state configuration $2p^6 3d^n$. Below, we shall refer to this effect for brevity as re-emission. Strictly speaking, the excitation and subsequent emission in a resonant process must be treated as a single event; an extensive literature exists on this subject (see, e.g., Refs. [26–28]). The effect is the more pronounced the stronger the localization of involved states is. The peculiarity of our present spectra is that such typically resonance-like phenomenon as re-emission is observed in spite of high-energy (i.e. non-resonance) electronic excitation, with the excitation energy of nearly 4 KeV, apparently due to sufficiently high lifetime of an electron trapped in a highly localized vacant Cr 3d state. For the Co-intercalated systems, the effect is practically not observable. Assuming phenomenologically the participation of the lowest vacant Cr 3d states in the X-ray emission, we leave the (otherwise single-particle) quantitative treatment of the spectrum till next section where the microscopic information about the electronic structure becomes available.

Another important observation concerning the X-ray emission spectra is a substantial increase – especially at low intercalant concentrations – of the L_β/L_α intensity ratio as compared to that in the pure metal. To our opinion, this indicates a localization of the 3d electron density and hence a magnetic moment. L_α and L_β bands originate from the dipole transitions $2p_{3/2}\rightarrow 3d_{5/2,3/2}$ and $2p_{1/2}\rightarrow 3d_{3/2}$, correspondingly. The change in the L_β/L_α relative intensity may be influenced by the selection rule on the total moment projection, $\Delta m_j = 0$, which in the present case favors a substantial decrease of the statistical weight of the $2p_{3/2}\rightarrow 3d_{5/2,3/2}$ transition, since the exchange interaction energy of 3d electrons (2–2.5 eV) by more than an order of magnitude exceeds their spin-orbit interaction energy.

As already mentioned above, the changes in the observed L_β/L_α weights distribution for systems with lower Cr content is opposite to what one could expect from the Coster-Kronig transitions, which redistribute intensities from $2p_{1/2}$ to the $2p_{3/2}$ channel. This indicates a relative unrelevance of the Coster-Kronig effect for the systems in question.

V. ELECTRONIC STRUCTURE CALCULATIONS

In Ref. [29] we reported the results of a first-principles optimization of lattice parameters in pure $TiSe_2$ (as well as in $TiTe_2$) and the electronic structure of 3d-intercalated systems, with the use of $M(TiSe_2)_3$ supercells in the latter case. The calculation has been done with the full-potential linearized augmented plane wave code WIEN97 [30], using the generalized gradient approximation (GGA) in the formulation by Perdew, Burke and Ernzerhof [31]. The hexagonal lattice parameters as found in the course of total energy minimization were a=3.519 Å, c=6.280 Å, whereas the experimental measurements give the values a=3.535 Å, c=6.004 Å (as cited in Ref. [32]). The internal coordinate z (the relative distance between Ti and Se layers) is 0.247 in the calculation, compared to the measured value of 0.25. At a first sight, the GGA overestimates the c/a ratio by as much as 5%. However, considering the reduced value of z in the calculation, one can notice that in reality just the van der Waals gap between adjacent chalcogen planes is overestimated, whereas the lenghts of Ti-Ti and Ti-Se bonds remain well within 1% of the experimental estimate. The Perdew–Burke–Ernzerhof formula for gradient approximation was optimally tuned for a certain degree of localization of the exchange-correlation hole, typical for bulk solids but not for the "empty" van der Waals gap. Some discussion on this subject can be found, e.g., in Ref. [33]. In the present study, we consider systems with relatively high concentration (1/3 per $TiSe_2$ unit) of intercalant atoms in the van der Waals gap, therefore the abovementioned shortcoming of the GGA treatment must be less serious than for pure dichalcogenides.

As in Ref. [29], we simulated intercalated systems using the rhombohedral $M(TiSe_2)_3$ supercell, shown in Fig. 8 (in the hexagonal setting). Similar supercells were earlier used in non-magnetic calculations by Suzuki *et al.* [34,35]. With only one type of supercell being considered in *ab initio* calculations, it had little sense to address the systematical trends in the lattice parameters under doping. Instead, we concentrated in our analysis on the properties of two intercalated systems as *impurity* systems. The calculations have been performed therefore in a fixed (c, a) frame, with a local atomic relaxation around the M atoms taken into account. This allows us to make a more clear comparison of Cr- and Co-intercalated systems. From the following it becomes obvious that the noticeably perturbed region around an intercalant atom is indeed much smaller than the region defined by the translation vectors in the supercell of our choice.

In the hexagonal setting, the supercell with the lattice constants $a' = a\sqrt{3}$, $c' = 3c$ (Fig. 8) hosts three $M(TiSe_2)_3$ units with the following atomic positions in one of them: M at (0,0,0); Ti at $(0, 0, \frac{1}{2})$ and at $\pm(0, 0, \frac{1}{6}+\Delta_1)$; six Se at $\pm(1-\Delta_2-\Delta_3, \frac{1}{3}-\Delta_3, \frac{5}{12}+\Delta_4)$; $\pm(\frac{2}{3}+\Delta_3, \frac{2}{3}-\Delta_2, \frac{5}{12}+\Delta_4)$; $\pm(\frac{1}{3}+\Delta_2, \Delta_2+\Delta_3, \frac{5}{12}+\Delta_4)$. The optimized values of internal coordinates Δ_1 to Δ_4, obtained from the condition that the forces on all atoms disappear, are listed in Table II. The local structural distortion, as compared to the equilibrium structure of $TiSe_2$, is quite small. The negative value of Δ_4 corresponds to the displacement of the chalcogen planes towards the Ti layers by 0.42% of the c parameter of $TiSe_2$; this corresponds roughly to $z = 0.247$ rather than 0.25 found for pure $TiSe_2$. A qualitative difference between $Cr_{1/3}TiSe_2$ and $Co_{1/3}TiSe_2$ is that the nearest Ti atoms approach the Co atom (Δ_1 slightly negative) but are shifted away from the Cr atom. This is consistent with the evidence of larger Co–Ti bonding and, contrarily, higher localization of the Cr3d states as addressed below.

The spatial distribution of the charge density in a plane cut across the supercell is shown in Fig. 9. The vertical size of the plot covers 18.84 Å. One can see that in the absence of an M atom the charge density between the Se layers is indeed rather low, about 0.05 e/Å^3. An intercalant atom embedded in this region mediates the chemical bonding between chalcogen atoms. An effectively larger (see below) Co atom provides a slightly higher charge density along the Se–M line. Moreover, the distrubution of the charge density along [001] (i.e., towards the nearest Ti atoms) is somehow different in Cr- and Co-intercalated crystals (Fig. 10). On the Co site, the occupation of 3d states is substantially higher as compared to Cr, with the effect that the effective size of an intercalant atom is larger, in spite of a slightly higher contraction of the Co3d states. At the same time, the occupation of the Ti3d shell is lower in the vicinity of Co next to a Cr atom. The local DOS distribution on the atoms in question (Fig. 11) helps to understand the origins and energetics of this different charge distribution.

The center of gravity of the Cr3d states lies closer to that of Ti3d. In spite of large exchange splitting at the Cr site, a noticeable contribution from both atoms is present near the Fermi level. Specifically, mostly the $3d_{z^2}$ orbitals at both Cr and Ti sites are responsible for this direct hybridization and the enhancement of the Ti DOS (of the atoms neighboring to Cr in the [001] direction) near the Fermi energy. This factor is not important in the Co-intercalated system because the Co3d states are lower in energy and do not mix so efficiently with Ti3d – in fact, the majority-spin band at the Co site is fully occupied. Apart from this enhancement of the direct Cr–Ti bonding, the distribution of electronic density (spatial as well as energy-resolved) within the $TiSe_2$ remains largely unaffected by the presence of intercalant atoms and very much close to that of pure $TiSe_2$ (see Ref. [36]. We notice however a difference of our electronic structure from that calculated for $TiSe_2$ in Ref. [32], with the use of the muffin-tin approximation).

The local DOS at the M site contains spin-splitted and broadened levels, typical for a magnetic impurity embedded in the VB (the latter being formed, in this case, by the Ti3d–Se4p hybridization). An anomalously narrow minority-spin peak appears at the Co site because its energy position is between the separated subbands due to a bonding and antibonding Ti–Se interaction (see more detailed discussion in Ref. [36]), i.e. the scattering of valence-band electrons at this impurity level is suppressed. A more detailed analysis of the crystal-field splitting and spatial distribution of the M3d orbitals will be given elsewhere [37]. It should be noted that the present calculation for the ordered $Cr_{1/3}TiSe_2$ structure failed to find an energy gap at the Fermi level (implied by the conductivity type as shown in Fig. 3 for x=0.33). The reason may be either an effect of the lattice parameters' change, important for the Cr-intercalated systems but ignored in the present calculation, or the importance of correlation effects due to high Cr3d localization, that would justify the use of a different (orbital-dependent) form of the total energy functional. This subject yet needs a further clarification.

The values of local magnetic moments (attributed to muffin-tin sphere sizes cited above) are 2.81 μ_B for Cr and 1.46 μ_B for Co, that agrees well with the experimental values of Table I for x=0.33. In spite of a slight variation of the magnetic density over the crystal (small antiparallel polarization of Ti3d shells and parallel of the Se4p shells), the magnetic moment remains quite localized at the intercalant atom. For the values of the 2p exchange splitting (taken simply as energy differences between spin-up and spin-down components of self-consistently calculated relativistic core levels), we obtained 0.85 eV at the Cr site and 0.59 eV at the Co site. The former is in good agreement with the experimental estimate, and the latter is probably already too small to be resolved with the experimental resolution (see Fig. 5).

With the information about the local state density distribution at intercalant sites available, it becomes possible to address the problem of X-ray re-emission in the Cr_xTiSe_2 systems with low x content. An assumption of a strongly localized character of Cr3d states is supported by the calculations of both spatial distribution (Fig. 9) and the local DOS (Fig. 11). Localized states in the vacant region (which may host an absorbed electron in an intermediate state of a X-ray emission process) must be necessarily those in the minority-spin channel. In order to imitate their possible participation in the X-ray re-emission, we calculated the Cr$L_{\alpha,\beta}$ X-ray emission spectrum, taking into account dipole transition matrix elements and the cutoff energy of 2 eV above the nominal Fermi level, to allow the lowest minority-spin band localized at the Cr site to contribute in full. This band incorporates more than two extra electrons, rather than one as would be the case in a simple intermediate-state model. However, there is no simple criterium to select

only part of these low-lying vacant states for their possible contribution to the re-emission process. The result of a calculation is shown in Fig. 7, top curve. Without the Fermi energy artificially shifted, the higher peak in both L_α and L_β bands is missing, so that the calculated spectrum is rather close to that of pure chromium. No such artificial adjustment was necessary for the Co_xTiSe_2 system.

CONCLUSION

As a result of this combined study incorporating measurements of the crystal structure, kinetic properties (conductivity) and the analysis of the electronic structure by different spectroscopic techniques (XPS and XES), interpreted on the basis of electronic structrure calculations, we establish the following. In spite of nominally identical magnetic moments of a free ion for Cr and Co, the saturation magnetization of intercalated $TiSe_2$ reveals an almost two times larger effective moment on Cr than that on Co sites. A large exchange splitting in the Cr3*d* shell polarizes the Cr2*p* shell and leads to the exchange splitting of Cr2*p* core levels large enough (0.9 eV) to be detected by photoelectron spectroscopy. No such splitting was resloved for Co2*p* levels. So different magnetic behavior can be traced to different strength of chemical bonding in Cr- and Co-intercalated systems. The bonding is stronger in Co_xTiSe_2, as is evidenced by larger distortion of the host lattice. The Cr3*d* states, on the contrary, remain more localized, that favors a higher magnetic moment. Another indication of higher localization of Cr3*d* states in Cr_xTiSe_2 is a strong contribution in the X-ray emission $L_{\alpha,\beta}$ spectrum from above the nominal Fermi level, observed even at excitation energies much higher than the threshold and tentatively attributed to re-emission. We emphasize that the exchange splitting of 2*p* core levels and a strong re-emission due to high-energy electronic excitations are experimental findings quite rarely observed in 3*d*-based systems so far. The reported first-principles calculations provide an adequate description of the structural and magnetic properties and simplify at least a qualitative understanding of the underlying physics. However, an attempt to take into account correlation effects more systematically could be interesting for the treatment of highly localized Cr3*d* states and of the excitation processes involving the latter.

ACKNOWLEDGMENT

This work was supported by the Russian Science Foundation for Fundamental Research (Projects 96-15-96598 and 99-03-32503), a NATO Linkage Grant (HTECH.LG 971222) and a DFG-RFFI Project. Financial support from the Deutsche Forschungsgemeinschaft is greatly acknowledged.

---

[1] M. Inoue, M. Koyano, H. Negishi, Y. Ueda, and H. Sato, Phys. stat. solidi (b) **132**(1), 295 (1985).
[2] M. Koyano, H. Negishi, Y. Ueda, M. Sasaki, and M. Inoue, Phys. stat. solidi (b) **138**(2), 357 (1986).
[3] A. Fujimori, S. Suga, H. Negishi, and M. Inoue, Phys. Rev. B **38**(6), 3676 (1988).
[4] R. H. Friend and A. D. Yoffe, Adv. Phys. **36**(1), 1 (1987).
[5] T. Hibma, *Structural Aspects of Monovalent Cation Intercalates of Layered Dichalcogenides* (Academic Press, London – New York, 1982), pp. 285–313.
[6] Y. Tazuke and T. Takeyama, J. Phys. Soc. Japan **66**(3), 827 (1997).
[7] T. Yamasaki, N. Suzuki, and K. Motizuki, J. Phys. C: Solid State Phys. **20**(3), 395 (1987).
[8] Y. Arnaud, M. Chevreton, A. Ahouandjinou, M. Danot, and J. Rouxel, J. Solid State Chem. **18**(1), 9 (1976).
[9] V. G. Pleshchev, A. N. Titov, and A. V. Kuranov, Phys. Solid State **39**(9), 1442 (1997).
[10] A. N. Titov, Phys. Metals and Metallography **81**(6), 629 (1996).
[11] A. Titov, S. Titova, M. Neumann, V. Pleschov, Y. Yarmoshenko, L. Krasavin, A. Dolgoshein, and A. Kuranov, Mol. Cryst. Liq. Cryst. **311**, 161 (1998).
[12] J. A. Wilson, Phys stat. solidi (b) **1**(1), 11 (1978).
[13] M. F. Sykes and J. W. Essam, J. Math. Phys. **5**(8), 1117 (1964).
[14] W. Y. Liang, in *Physics and Chemistry of Electrons and Ions in Condensed Matter. Proceedings of the NATO Advanced Study Institute*, edited by J. V. Acrivos, N. F. Mott, and A. D. Yoffe (Reidel, Dordrecht, Netherlands, 1984), pp. 459–478.
[15] J. F. Moulder, W. F. Stickle, P. E. Sobol, and K. D. Bomben, *Handbook of X-ray Photoelectron Spectroscopy* (Perkin-Elmer Corporation, Eden Prairie, Minnesota, 1992).

[16] It is noteworthy that the corresponding spectra of 3*d*-intercalated titanium disulphides exhibit an opposite trend: the Ti2*p* binding energy decreases on intercalation, consistently with other physical properties of $M_x\mathrm{TiS}_2$ that may be well cast into a rigid-band model, see Ref. [1,2]. In TiS_2, the lattice is more rigid along the hexagonal axis direction (consistently with smaller width of the van der Waals gap) as compared to TiSe_2. Consequently, the formation of covalent bonds between titanium and intercalant atoms is more difficult in $M_x\mathrm{TiS}_2$; the electrons provided by the dopant enter the "rigid" conduction band.
[17] Y. M. Yarmoshenko, M. I. Katsnelson, E. I. Schreder, E. Z. Kurmaev, A. Ślebarski, S. Plogman, T. Schlathölter, J. Braun, and M. Neumann, Eur. Phys. J. B **2**(1), 1 (1998).
[18] S. Plogmann, T. Schlathölter, J. Braun, M. Neumann, Y. M. Yarmoshenko, M. V. Yablonskikh, E. I. Shreder, E. Z. Kurmaev, A. Wrona, and A. Ślebarski, Phys. Rev. B **60**(9), 6428 (1999).
[19] J. J. Yeh and I. Lindau, At. Data Nucl. Data Tables **32**(1), 1 (1985).
[20] A. N. Titov, Phys. Solid State **38**(10), 1709 (1996).
[21] S. M. Butorin, J.-H. Guo, M. Magnuson, P. Kuiper, and J. Nordgren, Phys. Rev. B **54**(7), 4405 (1996).
[22] S. M. Butorin, J.-H. Guo, M. Magnuson, and J. Nordgren, Phys. Rev. B **55**(7), 4242 (1997).
[23] J. Kawai, K. Nakajima, K. Maeda, and Y. Goshi, Adv. X-ray Anal. **35**, 1107 (1992).
[24] M. Magnuson, N. Wassdahl, and J. Nordgren, Phys. Rev. B **56**(19), 12238 (1997).
[25] M. V. Yablonskikh, V. I. Grebennikov, Y. M. Yarmoshenko, E. Z. Kurmaev, S. M. Butorin, L.-C. Duda, C. Sothe, T. Käämbre, M. Magnuson, J. Nordgren, S. Plogmann, and M. Neumann, *Magnetic circular dichroism in X-ray fluorescence of Heusler alloys at threshold excitation* (unpublished).
[26] Y. Ma, Phys. Rev. B **49**(9), 5799 (1994).
[27] J.-E. Rubensson, J. Lüning, S. Eisebitt, and W. Eberhardt, Appl. Phys. A **65**, 91 (1997).
[28] N. Mårtensson, M. Weinelt, O. Karis, M. Magnuson, N. Wassdahl, A. Nilsson, J. Stöhr, and M. Samant, Appl. Phys. A **65**, 159 (1997).
[29] A. V. Postnikov, M. Neumann, S. Plogmann, Y. M. Yarmoshenko, A. N. Titov, and A. V. Kuranov, *Magnetic properties of* 3*d-doped* $TiSe_2$ *and* $TiTe_2$ *intercalate compounds*, (to be published in Comput. Mater. Sci.).
[30] P. Blaha, K. Schwarz, and J. Luitz, *WIEN97, Vienna University of Technology* (1997), improved and updated Unix version of the original copyrighted WIEN-code, which was published by P. Blaha, K. Schwarz, P. Sorantin, and S. B. Trickey, in Comput. Phys. Commun. 59, 339 (1990).
[31] J. P. Perdew, K. Burke, and M. Ernzerhof, Phys. Rev. Lett. **77**(18), 3865 (1996); J. P. Perdew, K. Burke, and M. Ernzerhof, Phys. Rev. Lett. **78**(7), 1396 (1997); Y. Zhang and W. Yang, Phys. Rev. Lett. **80**(4), 890 (1998); J. P. Perdew, K. Burke, and M. Ernzerhof, Phys. Rev. Lett. **80**(4), 891 (1998).
[32] A. Leventi-Peetz, E. E. Krasovskii, and W. Schattke, Phys. Rev. B **51**(24), 17965 (1995).
[33] S. Tinte, M. G. Stachiotti, C. O. Rodriguez, D. L. Novikov, and N. E. Christensen, Phys. Rev. B **58**(18), 11959 (1998).
[34] N. Suzuki, T. Yamasaki, and K. Motizuki, J. Magn. Magn. Mater. **70**(1–3), 64 (1987).
[35] N. Suzuki, T. Yamasaki, and K. Motizuki, J. Phys. Soc. Japan **58**(9), 3280 (1989).
[36] Y.-S. Kim, M. Mizuno, I. Tanaka, and H. Adachi, Jpn. J. Appl. Phys. **37, Pt. 1**(9A), 4878 (1998).
[37] A. N. Titov, A. S. Ovchinnikov, and A. V. Kuranov, *The role of Me*3*d-Ti*3*d hybridization in the reduction of magnetic moments of intercalant ions* Co^{3+} *and* Cr^{3+} *in* $TiSe_2$ (unpublished).

TABLE I. Effective magnetic moment $\mu_{\mathrm{eff.}}$ (in μ_{B}) as measured for different intercalant concentrations

$x=$	0.10	0.20	0.25	0.33
$\mathrm{Co}_x\mathrm{TiSe}_2$	2.67	2.38	2.24	1.64
$\mathrm{Cr}_x\mathrm{TiSe}_2$	3.85	3.03	3.29	2.56

TABLE II. Internal coordinates in relaxed $M_{1/3}\mathrm{TiSe}_2$ supercells

M	$\Delta_1\times10^3$	$\Delta_2\times10^3$	$\Delta_3\times10^3$	$\Delta_4\times10^3$
Cr	0.26	1.89	0.47	−1.13
Co	−0.02	1.53	0.50	−1.40

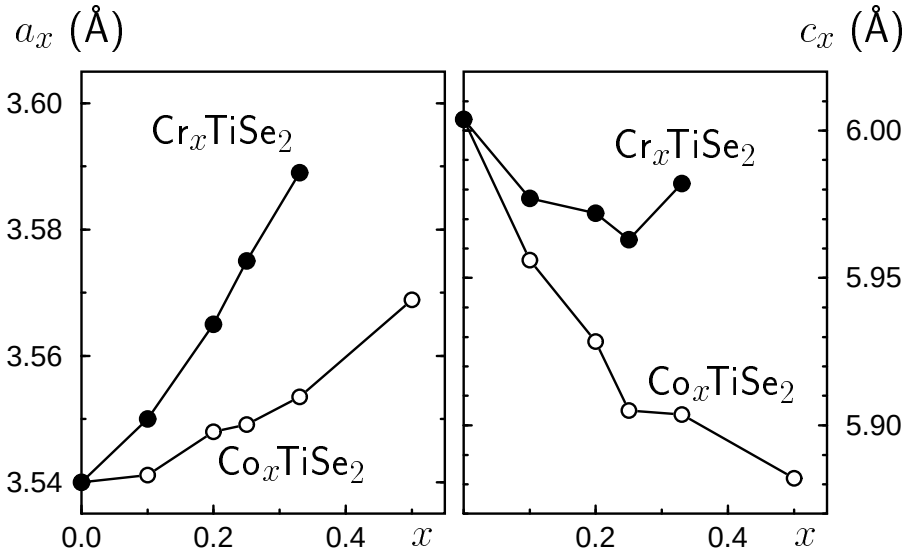

FIG. 1. The hexagonal unit cell parameters a and c of Co_xTiSe_2 and Cr_xTiSe_2 depending on x.

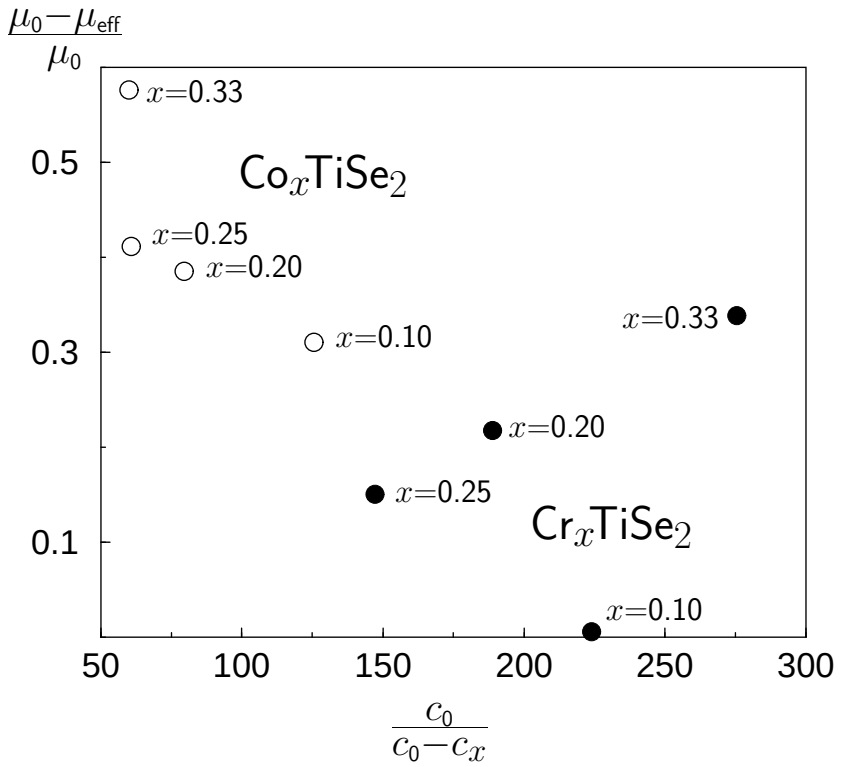

FIG. 2. Correlation between reduced magnetic moment of intercalant atom $\mu_0 - \mu_{\rm eff}/\mu_0$ (μ_0 is the nominal free ion magnetic moment, $\mu_{\rm eff}$ as determined from magnetic susceptibility measurements) and the lattice deformation parameter $c_0/(c_0 - c_x)$.

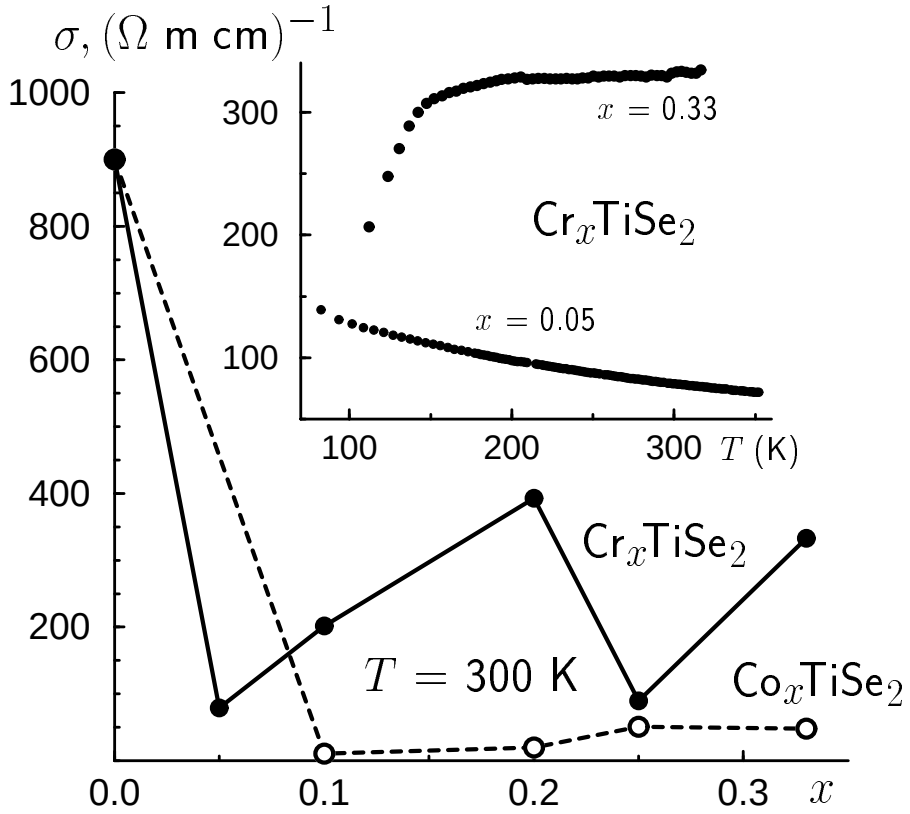

FIG. 3. The conductivity of Co_xTiSe_2 and Cr_xTiSe_2 as function of intercalant content at T=300 K. Inset: the temperature dependence of conductivity for Cr_xTiSe_2 with x=0.05 and 0.33.

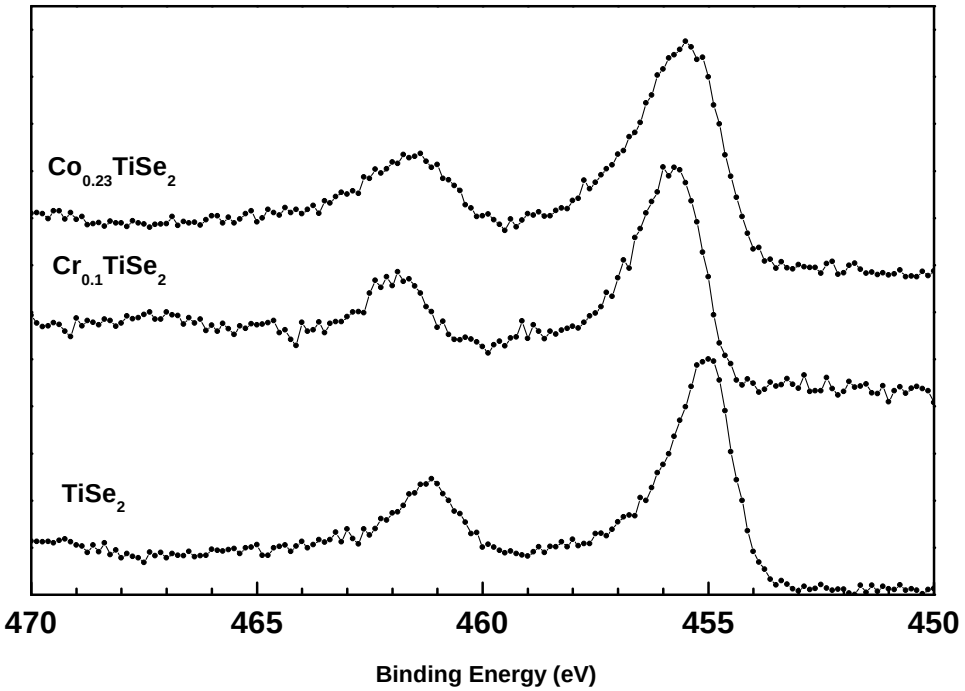

FIG. 4. X-ray photoelectron spectra of Ti 2p core levels in $Co_{0.23}TiSe_2$, $Cr_{0.1}TiSe_2$, and $TiSe_2$.

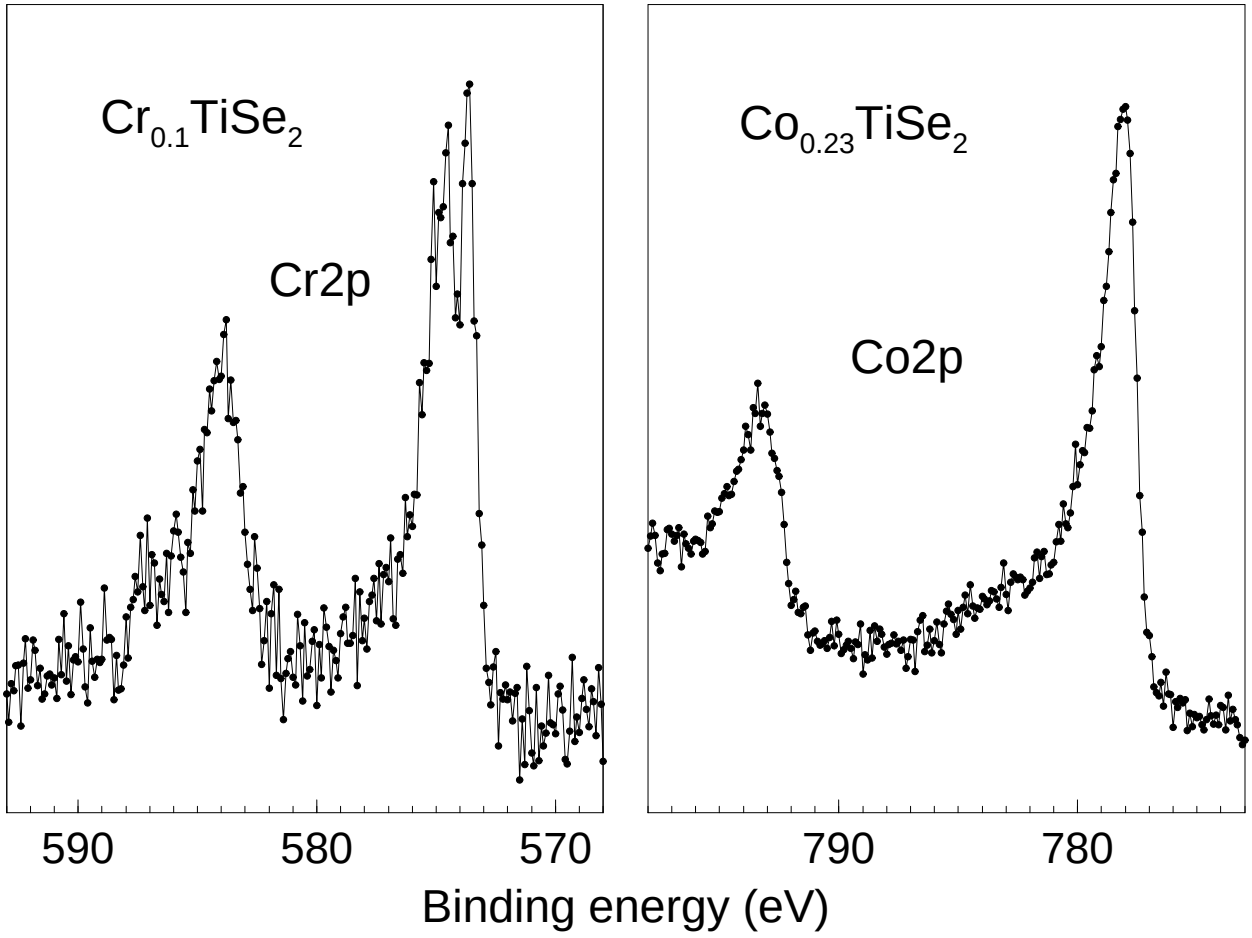

FIG. 5. X-ray photoelectron spectra of intercalant $2p$ core levels in $Cr_{0.1}TiSe_2$ and $Co_{0.23}TiSe_2$.

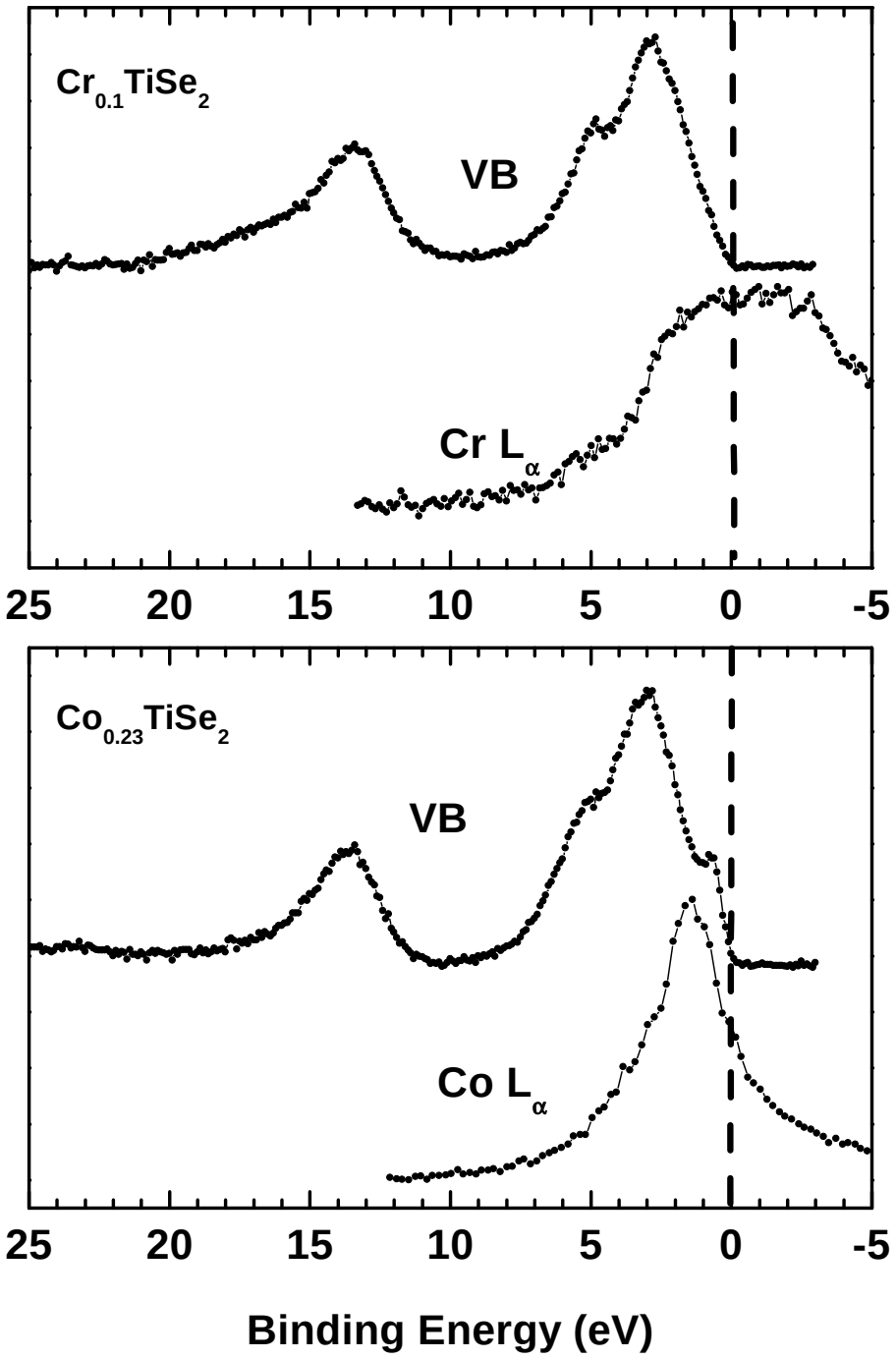

FIG. 6. X-ray photoelectron spectrum of the valence band (VB) and L_α X-ray emissioum, brought into the same scale of binding energies for $Co_{0.1}TiSe_2$ (top panel) and $Cr_{0.23}TiSe_2$ (bottom panel). Note the contribution to the CrL_α spectrum from the states above the Fermi energy.

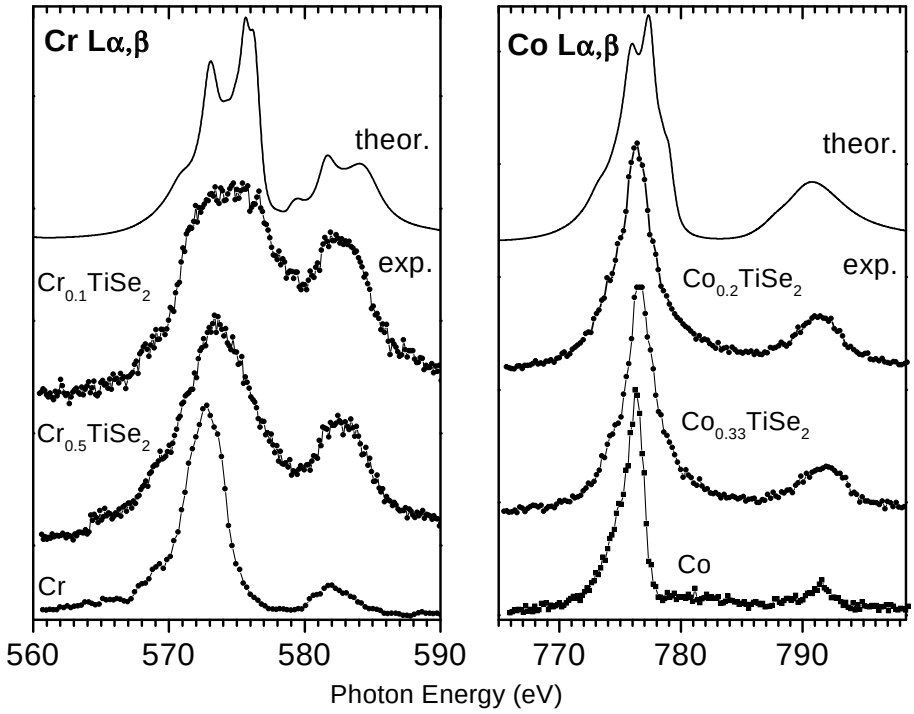

FIG. 7. $L_{\alpha,\beta}$ X-ray emission spectra of Cr and Co in pure metals (bottom) and intercalated $TiSe_2$. Top curve: the spectra calculated from first principles for the $M(TiSe_2)_3$ (M=Cr, Co) supercell; see text for details.

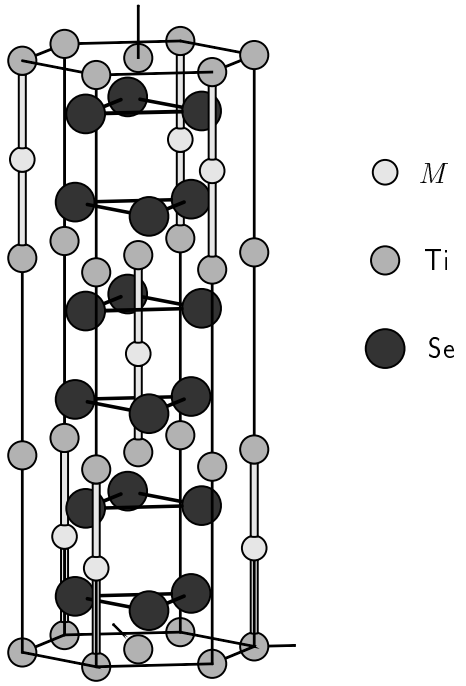

FIG. 8. The $M(TiSe_2)_3$ supercell (in the hexagonal setting) used in the *ab initio* electronic structure calculations (M=Cr, Co).

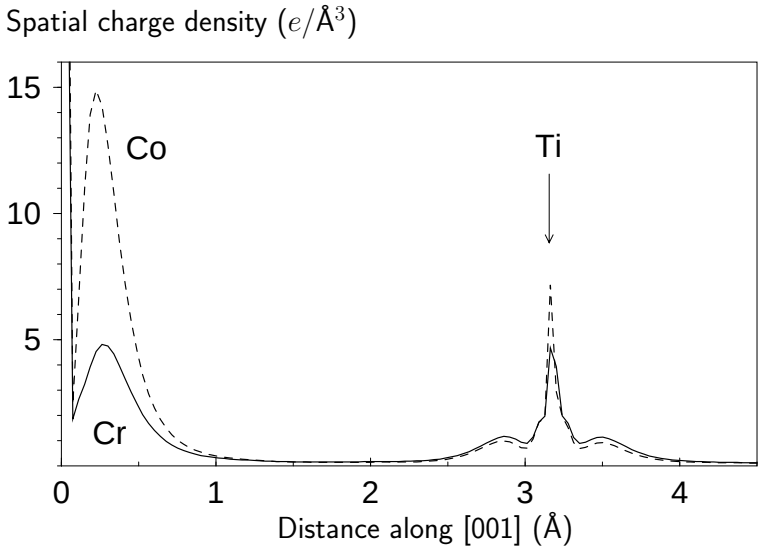

FIG. 9. The cut of the charge density distrubution along the [001] from the M position in $M(TiSe_2)_3$ (M = Cr, Co).

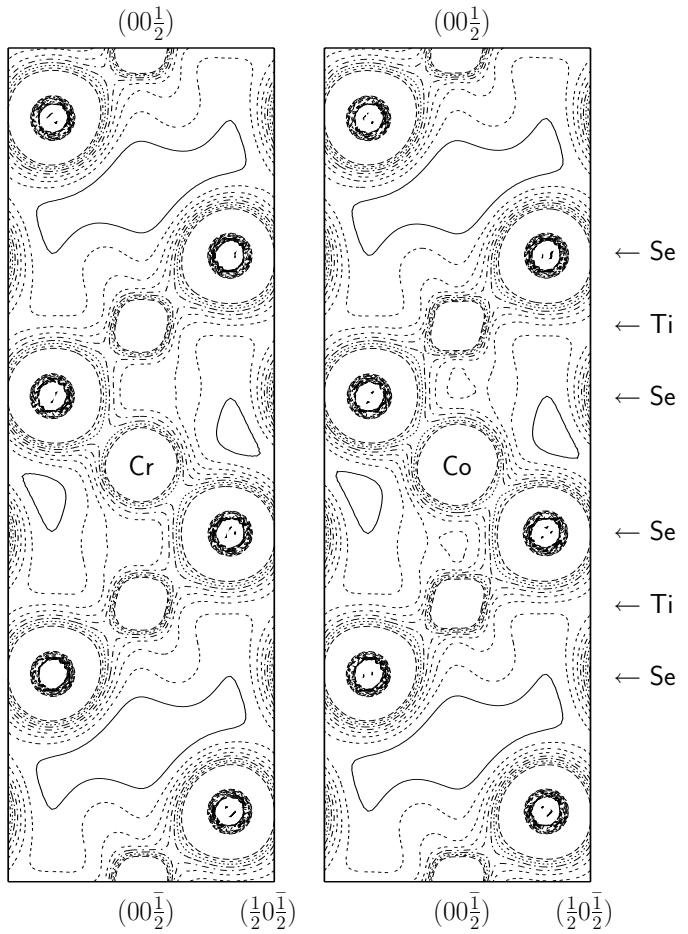

FIG. 10. The contour plot of the charge density distrubution over the supercell. The points labeled are in the supercell hexagonal setting ($c' = 3c$, $a' = \sqrt{3}a$ – see text). The contours go up to 0.5 e/Å^3 with the step 0.05 e/Å^3.

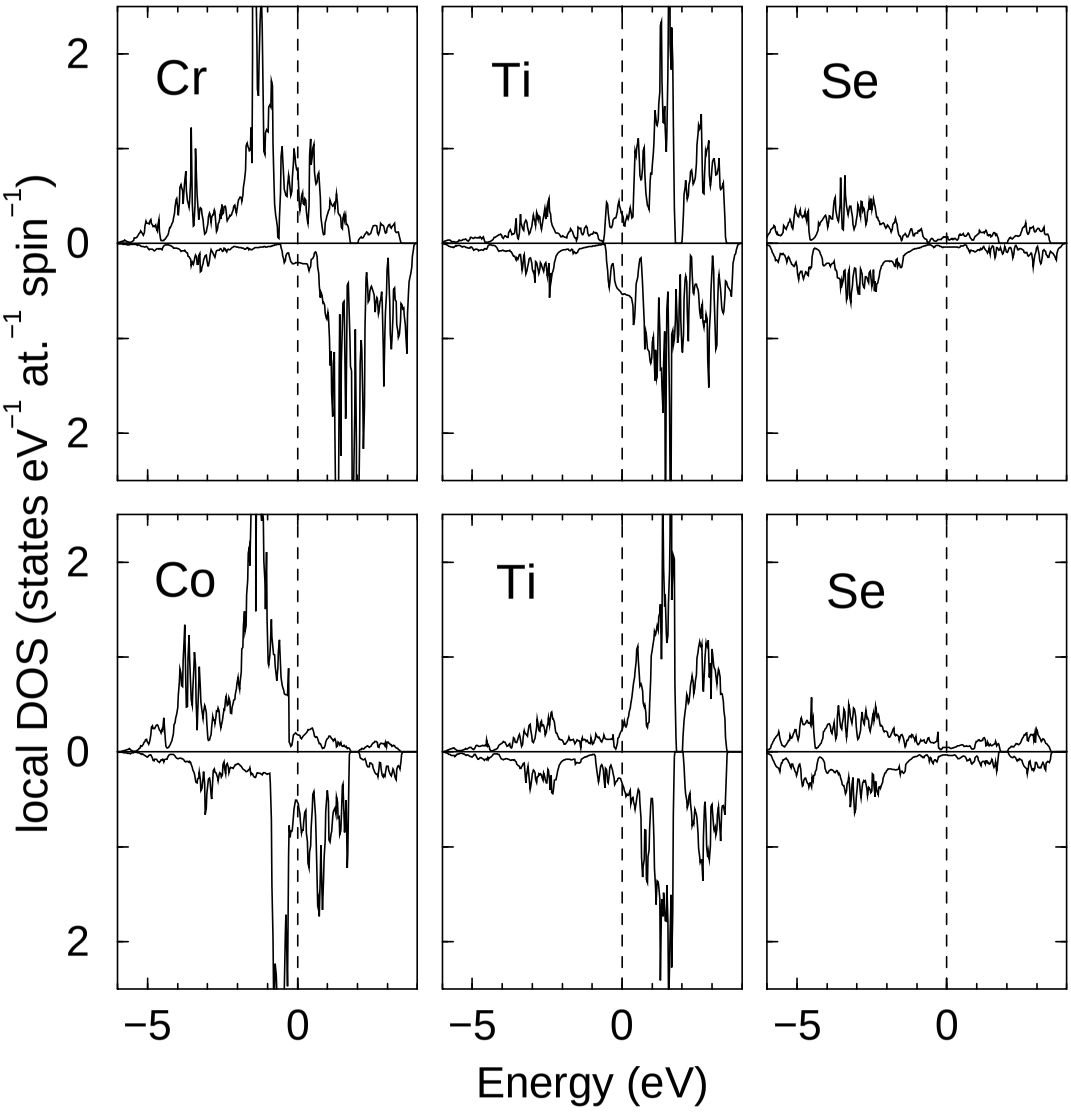

FIG. 11. $M3d$, Ti3d (at the Ti atoms closest to M), and Se4p-DOS as calculated for the $M(TiSe_2)_3$ supercell. Upper row: M = Cr, lower row: M = Co.